Lifetimes of ^{32}P levels

A. Kangasmäki,* P. Tikkanen, and J. Keinonen
Accelerator Laboratory, P.O. Box 43, FIN-00014, University of Helsinki, Finland

W. E. Ormand
INFN sezione di Milano, via Celoria 16, 20133 Milano, Italy
and Oak Ridge National Laboratory, Oak Ridge, Tennessee 37831

S. Raman
Oak Ridge National Laboratory, Oak Ridge, Tennessee 37831
(Received 22 November 1996)

Mean lifetimes of 22 bound levels and upper lifetime limits of four more levels in ^{32}P below an excitation energy of 6.4 MeV were deduced from the Doppler-shift attenuation of γ rays produced in the inverse reaction ^{2}H(^{31}P,$p\gamma$). Of these 26 levels, the lifetimes of six levels are reported here for the first time. The low-lying portion of the level scheme, the level lifetimes, and the γ-ray branchings and reduced transition probabilities have been compared with shell-model predictions. The overall agreement is reasonably good. [S0556-2813(97)02904-X]

PACS number(s): 21.10.Tg, 23.20.−g, 27.30.+t

I. INTRODUCTION

In the case of the self-conjugate nucleus $^{28}_{14}$Si$_{14}$, it has been shown [1] that the shell-model level scheme calculated in the $0d_{5/2}\ 1s_{1/2}\ 0d_{3/2}$ space agrees reasonably well with experiments up to an excitation energy of 13 MeV. A more stringent test of model wave functions is provided by comparisons of electromagnetic observables and, in a recent study [2], one-third of the ~30 experimentally determined matrix elements in ^{28}Si for states above 6 MeV were found to be poorly reproduced (differing by a factor of 2 or more) by existing shell-model calculations. (Below 6 MeV, there are only three known excited states in ^{28}Si and three significant matrix elements.) To extend such comparisons to other *sd*-shell nuclei, a study of transition strengths in $^{32}_{16}$S$_{16}$ (another self-conjugate nucleus) was begun by means of the ^{31}P(p,γ), ^{28}Si(^{6}Li,$d\gamma$), and ^{2}H(^{31}P,$n\gamma$) reactions. During the analysis of the data from the last-mentioned reaction, it was noted that the competing ^{2}H(^{31}P,$p\gamma$) reaction leading to levels in $^{32}_{15}$P$_{17}$ was ~4 times stronger than the ^{2}H(^{31}P,$n\gamma$) reaction leading to levels in ^{32}S. Therefore, it was imperative that the data should be analyzed first to separate out the ^{32}P part. Lifetimes deduced from this analysis are reported in this paper.

Previously reported [3–11] lifetime values in ^{32}P are listed in Table I. Except for the 78-keV level, all lifetimes have been obtained using the Doppler-shift-attenuation (DSA) method. Table II lists the nuclear reactions used and contains a summary of the stopping conditions. As seen from Table I, the lifetimes of many levels above 2.5 MeV are either unknown or, if known, have large uncertainties. It is not surprising that previously measured values show wide variations because (i) targets with layered structures (that make DSA analysis complicated) were used (see Table II and Sec. II C) (ii) recoil velocities were quite low, and (iii) the stopping powers were in most cases small and poorly known. A systematic remeasurement of lifetimes is therefore warranted independent of any other reason. These results are reported in Sec. II.

During the last decade, untruncated *sd* shell-model calculations [12–14] have been fairly successful in reproducing a large body of spectroscopic data pertaining to the low-lying portion of the level schemes of several nuclei in the $18<A<38$ region. A comparison between experiment and calculation for ^{32}P is therefore of interest in determining the degree of this agreement. This comparison is made in Sec. III. Our conclusions are given in Sec. IV.

II. EXPERIMENT

A. Procedure

Lifetime measurements were carried out at the Accelerator Laboratory of the University of Helsinki using the ^{2}H(^{31}P,$p\gamma$)^{32}P reaction. This reaction dominates over the competing ^{2}H(^{31}P,$n\gamma$)^{32}S and ^{2}H(^{31}P,$\alpha\gamma$)^{29}Si reactions, and the level scheme of ^{32}P is simple enough such that singles measurements (with good statistics) were deemed sufficient. High recoil velocities (3.8–4.3 % of the velocity of light) produced during the aforementioned reaction guaranteed that the slowing down of recoiling ^{32}P nuclei took place at velocities at which the electronic stopping power (i) is experimentally known, (ii) is dominant relative to the nuclear stopping power, and (iii) is close to its maximum value.

For the current study, ^{31}P$^{4,5+}$ ion beams of 45–150 particle nA were supplied by the 5-MV tandem accelerator EGP-10-II. Bombarding energies of ~24 and ~29 MeV

*Electronic address: aki.kangasmaki@helsinki.fi

TABLE I. Lifetimes of levels in ^{32}P obtained in the current and previous works. In our notation, 520 $^{90}_{50}\equiv$ 520$^{+90}_{-50}$, 365 *36* $\equiv$ 365 $\pm$ 36, 3.00 *85* $\equiv$ 3.00 $\pm$ 0.85, etc.

Level	Previous work			Previous work	This work: ^{2}H(^{31}P,$p\gamma$)		
E_x [a]	Quoted	Quoted		Reanalyzed [b]	$E=24$ MeV	$E=29$ MeV	Adopted
(keV)	$F(\tau)$ (%)	τ	Ref.	τ	τ	τ	τ
78		520 $^{90}_{50}$ ps	[3] [c]		not measured		402 *13* ps
		365 *36* ps	[4] [d]				
		402 *13* ps	[6] [e]				
513	13.3 *25*	3.00 *85* ps	[5]	3.30 *83* ps	not measured		2.64 *12* ps
	2 *9*	$>$2 ps	[8]	$>$2.2 ps			
		2.64 *8* ps	[11]	2.64 *12*			
1149	67 *3*	270 *65* fs	[5]	300 *60* fs	255 *18* fs	271 *19* fs	264 *18* fs
	59.1 *56*	210 *44* fs	[7]	360[f] *110* fs			
	65.1 *29*		[7]	310[f] *90* fs			
	61 *8*	220 *60* fs	[8]	250 *80* fs			
		252 *8* fs	[11]	260 *20* fs			
1323	59.1 *15*	380 *80* fs	[5]	430 *80* fs	510 *35* fs	525 *45* fs	487 *25* fs
	39.8 *24*	580 *55* fs	[7]	710[f] *180* fs			
	47 *5*	350 *70* fs	[8]	400 *90* fs			
		472 *17* fs	[11]	472 *25* fs			
1755	50.3 *22*	510 *110* fs	[5]	590 *120* fs	600 *40* fs	635 *50* fs	621 *40* fs
	40.2 *24*	616 *55* fs	[7]	700 *180* fs			
	39 *3*	460 *70* fs	[8]	530 *100* fs			
		660 *50* fs	[11]	660 *50* fs			
2178	90.9 *26*	60 *25* fs	[5]	64 *23* fs	94 *16* fs	78 *15* fs	76 *14* fs
	86.2 *18*	91 *14* fs	[7]	98 *25* fs			
	91 *2*	52 *12* fs	[8]	57 *14* fs			
2218	71 *4*	210 *50* fs	[5]	230 *50* fs	260 *25* fs	200 *33* fs	240 *25* fs
	57.5 *51*	287 *24* fs	[7]	380 *100* fs			
	65.6 *33*		[7]	290 *80* fs			
	69 *8*	160 *50* fs	[8]	190 *60* fs			
2230	94.1 *25*	36 *20* fs	[5]	41 *21* fs	not measured		$<$50 fs
	96 *4*	$<$50 fs	[8]	$<$50 fs			
2657	101 *7*	$<$40 fs	[7]	$<$40 fs	11 *4* fs	14 *5* fs	12 *4* fs
	100.3 *8*	$<$10 fs	[8]	$<$10 fs			
2740	87 *8*	70 *40* fs	[8]	80 *45* fs	16 *7* fs	23 *7* fs	20 *7* fs
3005	86.0 *9*	87 *4* fs	[7]	97 *23* fs	108 *16* fs	103 *16* fs	101 *16* fs
	88.1 *9*		[7]	87 *21* fs			
	93 *2*	41 *12* fs	[8]	44 *13* fs			
3149	48.0 *19*	510 *36* fs	[7]	570 *140* fs	not measured		595 *110* fs
	35 *3*	530 *80* fs	[8]	610 *110* fs			
3264	75 *5*	130 *30* fs	[8]	145 *40* fs	190 *25* fs	147 *22* fs	164 *22* fs
	17 *5*	180 *70* fs	[10]	210 $^{100}_{60}$ fs			
3321	57.6 *12*	360 *14* fs	[7]	400 *100* fs	not measured		272 *50* fs
	62 *4*	210 *40* fs	[8]	240 *50* fs			

TABLE I. (*Continued*).

Level E_x [a] (keV)	Previous work Quoted $F(\tau)$ (%)	Quoted τ	Ref.	Previous work Reanalyzed [b] τ	This work: ^{2}H(^{31}P,$p\gamma$) $E=24$ MeV τ	$E=29$ MeV τ	Adopted τ
3443	44 *5*	380 *80* fs	[8]	440 *100* fs	365 *45* fs	400 *50* fs	387 *45* fs
3444	94.9 *17*	35 *14* fs	[7]	38 *15* fs	not measured		38 *15* fs
3792	not reported				5.4 *20* fs	6.0 *20* fs	5.7 *20* fs
3797	89.8 *53* 96 *16*	71 *38* fs $<$95 fs	[7] [9]	77 *43* fs $<$100 fs	not measured		77 *43* fs
3880	96.4 *27*	28 *22* fs	[7]	27 *19* fs	$<$20 fs	$<$20 fs	$<$20 fs
3990	101.9 *19* 97.0 *18*	$<$10 fs 18 *8* fs	[7] [9]	$<$10 fs 19 *11* fs	$<$15 fs	$<$15 fs	$<$15 fs
4009	not reported				160 *60* fs	200 *40* fs	188 *40* fs
4035	92 *6*	35 *25* fs	[9]	45 *30* fs	not measured		45 *30* fs
4036	90 *5*	4.1 *24* fs	[10]	5.1 *30* fs	$<$3 fs	2.1 *8* fs	2.1 *8* fs
4151	92.5 *26* 86 *12*	52 *20* fs 70 *50* fs	[7] [9]	55 *24* fs 70 *60* fs	28 *10* fs	26 *10* fs	30 *10* fs
4205	not reported				4.2 *11* fs	4.3 *12* fs	4.2 *11* fs
4275	25 *3*	770 *120* fs	[9]	870 *160* fs	not measured		870 *160* fs
4313	83 *10*	80 *40* fs	[9]	90 *50* fs	not measured		90 *50* fs
4411 [g]	not reported				14 *6* fs	20 *3* fs	19 *3* fs
4662	65 *54*	20 $^{250}_{20}$ fs	[10]	20 $^{250}_{20}$ fs	3.9 *8* fs	4.0 *7* fs	4.0 *7* fs
4743	60[h] *10*	140 *40* fs	[9]	160[h] *70* fs	not measured		160 *70* fs
4877	107 *14*	$<$3 fs	[10]	$<$3 fs	4.5 *13* fs	6.6 *11* fs	5.7 *11* fs
5081	69 *10*	150 *50* fs	[9]	170 *70* fs	not measured		170 *70* fs
5253	91 *9*	$<$85 fs	[9]	$<$90 fs	not measured		$<$90 fs
5350	68 *36*	16 $^{51}_{16}$ fs	[10]	16 $^{51}_{16}$ fs	8.0 *9* fs	7.1 *9* fs	7.6 *9* fs
5509	not reported				10.2 *20* fs	10.3 *15* fs	10.3 *15* fs
5779	83 *22*	6 $^{12}_{6}$ fs	[10]	5 $^{12}_{5}$ fs	1.5 *7* fs	$<$3 fs	1.5 *7* fs
6062	not reported				$<$5 fs	1.5 *6* fs	1.5 *6* fs
6196	not reported					$<$5 fs	$<$5 fs
6333	not reported					$<$5 fs	$<$5 fs

[a]Excitation energies for the levels at 2178, 2657, 3321, 3792, 3797, 4151, 4411, and 4662 keV are from Ref. [35] in combination with Ref. [34]; all others from Ref. [34].

[b]The $F(\tau)$ values reported in the literature were reanalyzed in this work. The resulting lifetime values are listed. For details, see Sec. II C.

[c]Proton-γ delayed-coincidence measurement in the ^{31}P($d,p\gamma$) reaction.

[d]Delayed coincidence in the ^{31}P(thermal n,γ) reaction.

[e]Recoil distance measurement with the ^{29}Si($\alpha,p\gamma$) reaction.

[f]Because the feeding fractions are not given in the original paper, these values are really upper limits.

[g]Up to 4.4 MeV, all known levels are listed, above only those for which there exist lifetime data.

[h]The reanalyzed lifetime value is based on an $F(\tau)$ value of 70% instead of the quoted 60%, because there is an apparent misprint in the original paper. The latter $F(\tau)$ value would yield a revised lifetime value of 220 $\pm$ 60 fs.

TABLE II. Summary of the experimental conditions and analysis procedures used in the lifetime measurements of ^{32}P levels using the Doppler-shift-attenuation (DSA) method.

Ref.	Reaction v/c(%)	(i) Slowing-down medium. (ii) DSA analysis.
Current	^{2}H(^{31}P,$p\gamma$)	(i) Gold implanted with ^{20}Ne (3.1×10^{16} atoms/cm^2) and ^{2}H (6.2×10^{17} atoms/cm^2), and silicon implanted with ^{2}H (6.2×10^{18} atoms/cm^2).
	3.8–4.3	(ii) Experimental stopping power as described in the text. Computer simulation of the slowing down and experimental conditions. Uncertainty of the stopping power included. Doppler-broadened line-shape analysis.
[5]	^{29}Si($\alpha,p\gamma$)	(i) Evaporated $^{29}SiO_2$ (100 or 240 μg/cm^2) on carbon (230 μg/cm^2).
	0.7–1.0	(ii) Nuclear stopping power described according to the Blaugrund formalism [50] using an analytic approximation for the LSS nuclear stopping cross section [49]. The electronic stopping power from the LSS theory corrected by $f_e=1.0+24.3v/c$, based on measurements of Ormrod, MacDonald, and Duckworth [Can. J. Phys. **43**, 275 (1963)]. Targets tilted 45° relative to beam for $v/c>0.8\%$. Identical stopping powers for SiO_2 and carbon assumed. A 20% uncertainty in the stopping power included. $F(\tau)$ analysis.
[7]	^{29}Si($\alpha,p\gamma$)	(i) $^{29}SiO_2$ (700 and 990 μg/cm^2) on gold.
	0.80, 0.87	(ii) LSS and Blaugrund. Slowing down in the target and target substrate taken into account. A 25% uncertainty in the stopping power assumed but not included in the quoted lifetime values. $F(\tau)$ analysis.
[8]	^{29}Si($\alpha,p\gamma$)	(i) Evaporated $^{29}SiO_2$ (184 μg/cm^2) on gold.
	1.4–1.5	(ii) LSS and Blaugrund. The LSS electronic stopping power was corrected by a factor quadratic in the ion velocity, based on interpolation of experimental data reported by Ormrod, MacDonald, and Duckworth [Can. J. Phys. **43**, 275 (1963)] and by Fastrup, Hvelplund, and Sautter [Mat. Fys. Medd. Dan. Vid. Selsk. **35** (10) (1966)] and on the compilation of Northcliffe and Schilling [Nucl. Data **A7**, 233 (1970)]. Slowing down in the target and target substrate taken into account. A 20% uncertainty in the electronic stopping power included. $F(\tau)$ analysis.
[9]	^{29}Si($\alpha,p\gamma$)	(i) Evaporated $^{29}SiO_2$ (100 μg/cm^2) on gold.
	1.7–1.8	(ii) LSS and Blaugrund. Similar procedure as in Ref. [8] (see previous item). A 10–30 % uncertainty in the stopping power included. $F(\tau)$ analysis.
[10]	^{31}P(thermal $n,\gamma\gamma$)	(i) Red phosphorus.
	$\sim$0.01	(ii) LSS and Blaugrund. Recoil velocities are caused by the primary γ-ray emission. γ-γ coincidences measured between primary and secondary γ rays. $F(\tau)$ analysis.
[11]	^{2}H(^{31}P,$p\gamma$)	(i) Evaporated Ti (218–260 μg/cm^2) on Cu, Ag, or Au and then hydrated Ti to TiD in a deuterium atmosphere.
	5.8	(ii) Stopping power parametrized as $S(v)=S_n(v)+S_e(v)$, where the nuclear stopping power is $S_n(v)=1.26K_n^{\mathrm{Bohr}}(v/v_0)^{-1}$ with K_n^{Bohr} equal to the Bohr estimate at $v=v_0=c/137$ (c is the velocity of light) [Bohr, Dan. Vidensk. Selsk. Mat.-Fys. Medd. **18**, (8) (1948)]. Electronic stopping power described by $S_e(v)=a_0(v/v_0)[1+a_1(v/v_0)+a_2(v/v_0)^2+a_3(v/v_0)^3]^{-1}$ with the parameters ($a_0\ldots a_3$) fitted to experimental data of Ref. [38] between $2.5v_0$ and $12.7v_0$. For $v<2.5v_0$, electronic stopping power linearly interpolated to zero at $v=0$. A 5% uncertainty in the electronic stopping power included. Slowing down in the target not considered. Doppler-broadened line-shape analysis.

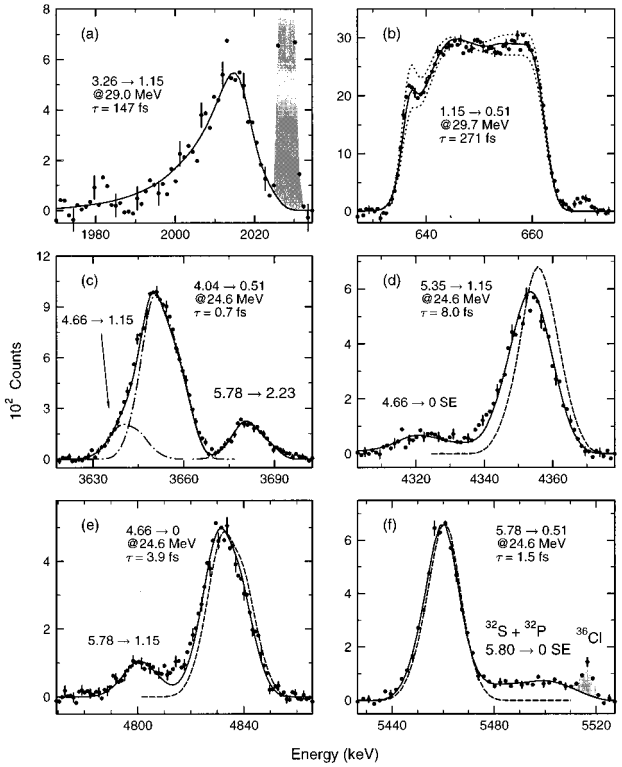

FIG. 1. Selected portions of background-corrected γ-ray spectra recorded in the ^{2}H(^{31}P,$p\gamma$)^{32}P reaction measurements with deuterium implanted in silicon (a) and gold (b)–(f). The γ-ray transitions and the energies of the bombarding ^{31}P beam are denoted in the figures (SE = single-escape peak). The solid lines illustrate the simulated best-fit line shapes corresponding to the lifetimes shown in Table I. The dotted lines in (b) demonstrate the change in the line shape due to a ± 25 fs change in the lifetime. The dot-dashed lines in (c) show each contributing transition separately. Line shapes corresponding to a lifetime of $\tau \ll 1$ fs shown by dashed lines in (d)–(f) represent the effects of reaction kinematics. The gray-shaded background peaks in (a) and (f) result from the competing ^{2}H(^{31}P,$\alpha\gamma$)^{29}Si reaction and the ^{35}Cl(thermal n,γ)^{36}Cl calibration source (see Sec. II A), respectively.

were chosen to optimize the yield from ^{32}P levels and to monitor the effects of feeding transitions on the γ-ray line shapes. Measurements at 20 MeV failed to produce useful results because of the much smaller yield of the reaction.

The beams were focused onto a 2×2 mm^2 spot on the target that was set with its surface perpendicular to the beam direction. The stainless-steel target holder was air cooled. Carbon buildup on the target surface was kept to a minimum by (i) the heat generated by the bombarding ion beam and (ii) by maintaining a vacuum better than 2 μPa in the target chamber.

The deuterium targets with high stopping powers, essential to the measurement of short lifetimes, were prepared by first implanting 100-keV ^{20}Ne$^+$ (3.1×10^{16} ions/cm^2) and then 45-keV ^{2}H$_3^+$ molecular ions (6.2×10^{17} atoms/cm^2) into 1.0-mm-thick gold sheets with a 120-keV isotope separator. The ^{20}Ne implantation provides trapping sites for ^{2}H and prevents its diffusion [15,16]. A low-stopping-power target (for deducing the initial recoil velocity distribution) was prepared by implanting 30-keV ^{2}H$_3^+$ molecular ions (6.2×10^{18} atoms/cm^2) into a 0.3-mm-thick, high-purity, crystalline silicon wafer. Changes in the γ-ray yields and line shapes of strong transitions were monitored during the DSA measurements in order to check the stability of deuterium implants under beam bombardment. Some loss of deuterium from the gold-backed targets was observed but the changes in the line shapes were found to be negligible. After the DSA measurements the targets were further checked by measuring the depth distributions of deuterium using the elastic recoil detection analysis (ERDA) method [17]. Previous studies [18] on implanted targets indicate that the implanted layer has no significant effect on the slowing down of ^{32}P recoils in gold and silicon and, hence, on the extracted lifetimes.

Slightly different bombarding energies were used (24.6 and 29.7 MeV for the gold-backed target, 24.0 and 29.0 MeV for the silicon-backed target) to ensure approximately equal center-of-mass energies for the ^{2}H(^{31}P,$p\gamma$)^{32}P reaction in both materials. At these bombarding energies, the average energy loss within the implantation depth was $\sim$1100 keV in gold and $\sim$320 keV in silicon.

The 40% efficient, high-purity Ge γ-ray spectrometer used in this work was operated in the escape-suppressed mode (in anticoincidence with a BGO annulus [2]) resulting in a suppression factor of $\sim$4. The energy resolution [full width at half maximum (FWHM)] of the spectrometer was 2.0, 3.1, 4.0, 4.6, and 5.1 keV at $E_\gamma = 1$, 3, 5, 7, and 9 MeV, respectively. The γ-ray spectra were accumulated in a 16 384 channel memory with a dispersion of 0.535 keV/channel.

The Ge detector was set so that its axis was aligned with the beam direction. The distance between the target and the closed end of the detector crystal was 55 mm. In this geometry, the solid angle of the crystal was 700 msr. A graded absorber (2.0 mm lead, 1.0 mm cadmium, and 1.5 mm copper) was inserted between the target and front face of the detector to reduce the high counting rate resulting from low-energy γ rays and x rays.

The efficiency calibration of the γ-ray spectrometer was performed with ^{56}Co and ^{66}Ga sources placed in the target position. Relative intensities of ^{56}Co γ rays for energies below 2.60 MeV were taken from Ref. [19] and for higher energies from Ref. [20]. The intensity values for the ^{66}Ga γ rays were given by Trzaska [21], who applied a correction factor to the original data of Refs. [22,23] for γ rays with energies $2 \leqslant E \leqslant 5$ MeV. This correction, suggested in Ref. [24], has been recently confirmed [25].

The dependence of the efficiency on the angle between the detector symmetry axis and the direction of γ-ray detection was measured using a collimated (1.5×1.5 mm^2) beam of ^{60}Co γ rays. Placed on a turntable, with the exit at the center and 55 mm from the detector crystal, the collimated source was rotated such that the detector efficiency response was mapped as a function of incident angle. The measured response was compared with the response calculated directly from the measuring geometry and detector dimensions, assuming that all γ rays hitting the detector are totally absorbed. Because of the good agreement between the measured and the calculated response, the latter one—

TABLE III. Experimental branching ratios for selected levels. In our notation, 47 *2* ≡ 47 ±2, 53.0 *22* ≡ 53.0 ±2.2, etc. All J^π assignments are from Ref. [34].

Initial state		Final state		Branching (%)	
E_x (keV)	J^π	E_x (keV)	J^π	Ref. [34]	Ref. [35]
2218	2^+	0	1^+	47 *2*	53.0 *22*
		78	2^+	12 *2*	12.1 *13*
		1149	1^+	9 *2*	11.1 *14*
		1323	2^+	32 *1*	24.0 *13*
3264	2^-	0	1^+	2.4 *2*	1.63 *24*
		78	2^+	12 *1*	12.6 *4*
		1149	1^+	46 *2*	47.8 *5*
		1323	2^+	18 *2*	16.85 *28*
		1755	3^+	11.7 *8*	12.64 *21*
		2230	1^+	10.3 *9*	8.47 *15*
4009	2^-	0	1^+	31 *3*	27.7 *15*
		78	2^+	27 *3*	24.2 *15*
		1149	1^+		5.7 *5*
		1323	2^+	4.2 *7*	6.7 *5*
		1755	3^+		6.9 *5*
		2178	3^+		1.85 *24*
		2218	2^+		2.03 *32*
		2579	(0–2)	5 *1*	
		2657	2^+		2.16 *35*
		3005	3^+		1.40 *20*
		3264	2^-	33 *4*	20.3 *9*
		3444	$(1,2^+)$		1.18 *17*
4151	3^-	78	2^+	75.9 *14*	71 *5*
		1755	3^+		4.9 *16*
		2178	3^+	<4	
		2218	2^+	10.8 *12*	6.9 *23*
		2657	2^+	13.3 *10*	12.2 *26*
		3264	2^-		5.5 *12*
		3149	4^+	<9	
5509	1^-	0	1^+	3.0 *2*	2.4 *5*
		78	2^+	8.4 *7*	
		1149	1^+	62 *4*	69.3 *16*
		2313 [a]	$(1^+–3^+)$	4.2 *3*	
		2740	1^+		2.2 *4*
		4036	1^-	23 *4*	20.0 *9*
		4205	1^+		6.1 *5*

[a]Spurious level according to Ref. [35].

corrected for the energy dependence of the γ-ray absorption—was used for other than ^{60}Co γ-ray energies.

The energy calibration of the spectrometer up to 8.6 MeV was performed using a ^{35}Cl(thermal n,γ)^{36}Cl [26] source which consisted of 10-kg NaCl surrounding an encapsulated ^{252}Cf fission source (about 10^5 neutrons/s). Neutrons were moderated to thermal energies in polyethylene sheets that were inserted between the fission source and NaCl. The γ-ray detector was shielded from fast fission neutrons by borated paraffin blocks. The ^{35}Cl(n,γ) ^{36}Cl source together with the ^{40}K laboratory background served also to monitor spectrometer stability. At a particular bombarding energy, a typical data set involved data from 10 runs of 2 h each that were summed together.

B. Analysis

Selected portions of γ-ray spectra are shown in Fig. 1. In the line-shape analysis of high-energy transitions ($E_\gamma \geq 2.7$ MeV) contents of adjacent channels were summed. The DSA analysis was performed by the computer simulation of γ-ray line shapes with the Monte Carlo (MC) method [27–33]. Using a 120-MHz Pentium-based personal computer, the line-shape analysis of a particular peak took only ~30 min if the peak represented a single γ ray from a level with a short lifetime. However, several days were required to fully analyze a peak if it was contaminated by a nearby peak (a transition of similar energy from a different level, an escape peak, etc.) in ^{32}P or ^{32}S or some other isotope. Altogether more than 50 peaks in ^{32}P were analyzed during this study.

The efficiency response of the γ-ray spectrometer was included in the simulations. The effect of the finite target thickness on the initial velocity of the recoiling ^{32}P nuclei was simulated in the DSA analysis by choosing the reaction depth randomly according to the ^{2}H depth distribution and taking into account the energy loss of the ^{31}P beam at that depth.

A simulated line shape was a sum of the shapes corresponding to the direct prompt and delayed feedings of a level. The sum was weighted by the experimental fractions of the feedings. These fractions were obtained from the measured population of the ^{32}P levels (at different bombarding energies) and from the γ-ray branching ratios reported in the literature [34] in combination with recent results [35] obtained from a detailed study of the ^{31}P(thermal n,γ) reaction. The experimental branching ratios for most of the levels listed in Table I are explicitly given in Tables III, IV, and V.

For most levels, the delayed feedings were observed to have an insignificant effect on the deduced lifetime values. Four levels that showed significant effects are discussed below. In deducing the lifetime value for the 1149-keV level, feeding fractions of (29.3 ±0.7)%, (1.0 ±0.3)%, and (0.9 ±0.3)% from the 3264-, 4009-, and 2218-keV levels, respectively, were used at the bombarding energy of ~24 MeV. At ~29 MeV, the corresponding fractions were (25.8 ±0.9)%, (1.0 ±0.3)%, and (1.1 ±0.3)%. Several other levels with short lifetimes and small feeding fractions do feed the 1149-keV level, but their effect on the deduced lifetime was found to be negligible. For the 3264-keV level, delayed feedings from the 4009-keV level with fractions of (5.0 ±0.6)% and (7.0 ±0.6)% at ~24- and ~29-MeV bombarding energies, respectively, were taken into account. At both bombarding energies, a fraction of (4.0 ±0.5)% from the 4151-keV level was used for the 2657-keV level and (5.0 ±0.6)% from the 5509-keV level for the 4036-keV level.

The observed line shape depends on the triple angular correlation between beam direction, emitted proton direction, and γ-ray-detection angle [36,37]. This relationship is most pronounced if the level lifetime is short ($\tau <$ 20 fs). Instead of including the full triple correlation in the simulation, a

TABLE IV. Comparison of experimental and calculated branching ratios and mixing ratios for positive-parity states in ^{32}P. Only those branchings that differ significantly from zero are given. All J^π assignments are from Ref. [34].

Initial state		Final state		Branching (%)		Mixing ratio $\delta(E2/M1)$[a]	
E_x (keV)	J^π	E_x (keV)	J^π	exp[b]	calc.	exp.	calc.
513	0^+	0	1^+	100	100		
1149	1^+	0	1^+	7.5 *7*	1.2		+0.73
		78	2^+	42.8 *13*	0.5	−0.14 *7*	+0.17
		513	0^+	50 *2*	98.3		
1323	2^+	0	1^+	59.4 *10*	49.7		+0.35
		78	2^+	40.6	49.7		−0.22
1755	3^+	0	1^+	2.1 *5*	0.01		
		78	2^+	95.9 *5*	97.7	+0.79 *8*	−0.40
		1323	2^+	2.0	2.2	+0.12 *10*	−0.01
2178	3^+	0	1^+	9.0 *9*	55.1		
		78	2^+	91.0	39.1	−0.14 *3*	−0.36
		1323	2^+	<3	1.7		−0.06
		1755	3^+	<1	3.8		−0.05
2218	2^+	0	1^+	53.0 *22*	9.8	+0.5 *2*	+0.95
		78	2^+	12.1 *13*	79.7		+0.04
		513	0^+		1.0		
		1149	1^+	11.1 *14*	1.6		+0.19
		1323	2^+	24.0 *13*	7.9	0.0 *3*	−0.07
2230	1^+	0	1^+	6 *1*	0.2		+4.16
		78	2^+	92	96.0		+0.21
		1149	1^+	<5	1.2		−0.37
		1323	2^+	1.9 *5*	2.4		−0.04
2657	2^+	0	1^+	69 *4*	47.5	−0.17 *3*	−0.10
		78	2^+	24 *4*	34.4		−0.09
		1149	1^+	<1	9.9		−0.12
		1323	2^+	<2	6.6		−0.07
		1755	3^+	7 *2*	0.7		−0.05
2740	1^+	0	1^+	27.4 *10*	10.8		−0.41
		78	2^+		51.0		+0.11
		513	0^+	71.0 *11*	36.2		
		1149	1^+	1.6 *3*	0.9		+0.27
		1323	2^+		1.0		−0.50
		1755	3^+		0.01		
		2178	3^+		<0.01		
3005	3^+	0	1^+	6.7 *6*	21.2		
		78	2^+	84.9 *8*	52.8		+0.41
		1149	1^+	<2	4.8		
		1323	2^+	4.4	14.8	+1.7 *8*	+0.56
		2178	3^+	4.0 *3*	3.3	+0.11 *16*	+0.39
		2218	2^+		2.5		−0.12
3149	4^+	78	2^+	7.1 *3*	10.5		
		1323	2^+	59.4 *6*	8.7		
		1755	3^+	13.4 *6*	71.7	+4.8 *12*	−0.22
		2178	3^+	20.2 *3*	9.2	+0.11 *4*	+0.08

TABLE IV. (*Continued*).

Initial state		Final state		Branching (%)		Mixing ratio $\delta(E2/M1)$	
E_x (keV)	J^π	E_x (keV)	J^π	exp	calc.	exp.	calc.
3444	$(1,2^+)$[c]	0	1^+	38 *3*	35.7		+0.29
		78	2^+	39 *3*	30.5		−0.07
		513	0^+	7 *1*	1.8		
		1149	1^+	<8	6.3		−1.32
		1323	2^+	<7	1.1		+0.67
		1755	2^+	<5	3.6		−0.005
		2218	2^+		3.9		+0.04
		2230	1^+	16 *3*	15.6		+0.05
		2657	2^+		1.4		+0.15
3792[d]	(1^+)	0	1^+		26.8		−0.16
		78	2^+	100	47.6		+0.08
		513	0^+		15.3		
		1323	2^+		3.6		+0.42
		2218	2^+		3.3		+0.07
		2230	1^+		2.4		+0.08
3797[d]	(3^+)	78	2^+	22.0 *12*	63.6	−0.6 *5*	−0.16
		1149	1^+	<2	1.5		
		1323	2^+	78.0 *12*	29.0	0.00 *3*	−0.13
		1755	3^+	<3	1.9		+0.02
		2218	2^+	<4	1.9		−0.08
3880	2^+	0	1^+	68 *5*	34.2		+0.16
		78	2^+	32 *5*	31.2		−0.35
		1149	1^+		7.9		−0.05
		1323	2^+		21.2		−0.13
		2230	1^+		1.1		+0.02
		2740	1^+		1.3		+0.004
3990	3^+	78	2^+	100	90.4		+0.03
		1323	2^+		4.8		+0.04
		2218	2^+		2.9		−0.29
4035	4^+	78	2^+	35 *2*	76.0		
		1323	2^+		5.2		
		1755	3^+	65 *2*	9.3	0.00 *3*	−0.28
		2178	3^+		1.3		+68.3
		3149	4^+		7.4		−0.02
4205	1^+	0	1^+		5.6		−0.78
		78	2^+	100	68.3		−0.02
		513	0^+		16.5		
		1323	2^+		2.7		−0.01
		2657	2^+		5.7		+0.05
4313	3^+	0	1^+		4.8		
		78	2^+	100	72.3		−0.11
		1149	1^+		3.6		
		1323	2^+		8.0		−0.07
		1755	3^+		7.5		−0.02
		2657	1^+		2.5		−0.08
4743	5^+	1755	3^+	<4	0.6		
		2178	3^+	28.7 *11*	31.8		
		3005	3^+	12.2 *11*	8.6		
		3149	4^+	46.8 *13*	50.7	+0.12 *4*	+0.09
		4035	4^+	12.3 *7*	8.3	+0.03 *5*	−0.005

[a]The sign convention of Rose and Brink [Rev. Mod. Phys. **39**, 306 (1967)] is used for the mixing ratios. The experimental values are from Ref. [34].

[b]Branching ratios for the levels at 2218, 2740, and 3792 keV are from Ref. [35]; all others from Ref. [34].

[c]A one-to-one correspondence between the experimental and calculated level schemes can be established only if spin-parity 2^+ is assigned to this state.

[d]In Ref. [34] the levels at 3792 and 3797 keV seen in (n,γ) and (d,p), respectively, are treated as a single level at 3793 keV. The branchings from these levels suggest that they are distinct.

TABLE V. Comparison of experimental and calculated branching ratios for negative-parity states. The two different calculations ($n=2$ or $n=3$, respectively, is the number of holes in the $0d_{5/2}$ orbit) are described in the text. Only those branchings that differ significantly from zero are given. All J^π assignments are from Ref. [34].

Initial state		Final state		Experimental	Calculated branching (%)	
E_x(keV)	J^π	E_x(keV)	J^π	branching[a] (%)	$n=2$	$n=3$
3264	2^-	0	1^+	1.63 *24*	0.1	23.4
		78	2^+	12.6 *4*	95.6	67.9
		1149	1^+	47.8 *5*	3.5	7.1
		1323	2^+	16.85 *28*		0.1
		1755	3^+	12.64 *21*	0.2	0.8
		2230	1^+	8.47 *15*	0.2	0.4
3321	3^-	78	2^+	75 *2*	65.9	97.2
		1323	2^+	25 *2*	27.7	
		1755	3^+	<4	3.0	0.2
		2178	3^+		1.2	1.4
		2218	2^+		1.0	
		2657	2^+		0.9	1.1
3443	4^-	1755	3^+	94.0 *12*	4.1	18.6
		2178	3^+	6.0 *12*	95.8	60.6
		3005	3^+		0.1	20.7
4009	2^-	0	1^+	27.7 *15*	68.1	85.2
		78	2^+	24.2 *15*	21.2	5.6
		1149	1^+	5.7 *5*	2.0	4.8
		1323	2^+	6.7 *5*	2.1	0.3
		1755	3^+	6.9 *5*	2.0	1.8
		2178	3^+	1.85 *24*		0.1
		2218	2^+	2.03 *32*	0.9	
		2230	1^+		3.4	1.9
		2657	2^+	2.16 *35*		0.2
		3005	3^+	1.40 *20*		0.2
		3264	2^-	20.3 *9*		
		3444	$(1,2^+)$	1.18 *17*		
4036	1^-	0	1^+	0.23 *2*	12.3	1.3
		78	2^+	3.2 *2*	6.7	0.1
		513	0^+	67 *3*	59.9	72.7
		1149	1^+	21 *3*	18.9	23.2
		1323	2^+	1.5 *2*	0.1	0.1
		2230	1^+	3.7 *9*	1.4	1.4
		2657	2^+	1.8 *5*	0.6	0.6
		3264	2^-	1.5 *4*		
4151	3^-	78	2^+	71 *5*	63.8	59.3
		1323	2^+		21.0	20.1
		1755	3^+	4.9 *16*	5.6	11.9
		2218	2^+	6.9 *23*	9.4	4.5
		2657	2^+	12.2 *26*	0.1	
		3264	2^-	5.5 *12*		
4275	5^-	3149	4^+	23 *12*		
		3443	4^-	77 *12*		
4411	0^-	0	1^+	87.2 *23*	2.2	98.5
		1149	1^+	12.8 *23*	94.6	1.2
		2740	1^+		2.4	0.3

TABLE V. (*Continued*).

Initial state		Final state		Experimental		Calculated branching (%)	
E_x(keV)	J^π	E_x(keV)	J^π	branching[a] (%)		$n=2$	$n=3$
4877	1^-	0	1^+	9.7	*6*	9.4	0.1
		78	2^+	2.8	*2*	3.8	41.8
		513	0^+	68	*1*	56.5	28.1
		1149	1^+			9.1	5.8
		1323	2^+	8.1	*5*	0.3	1.3
		2218	2^+			0.2	1.0
		2230	1^+			9.5	7.4
		2740	1^+	4.0	*6*	9.9	14.4
		3264	2^-	5	*1*		
		3444	2^+	2.1	*5*		

[a]Branching ratios for the levels at 3264, 4009, 4151, and 4411 keV are from Ref. [35]; all others from Ref. [34].

simplified approach was chosen: The correlation effect was described as an *effective* center-of-mass angular distribution of proton emission, which was determined from the line shape measured with the silicon-backed target. The triple angular correlation reduces to an ordinary angular distribution if the γ rays are observed with a point detector at 0° with respect to the beam direction [36]. Our setup approximates these conditions.

Because the effective angular distribution is not known initially, an iterative procedure is necessary. An isotropic angular distribution used for the simulation in gold yields the first approximation for the lifetime. This value is then used for the simulation of the angular distribution in silicon. The distribution is adjusted until the χ^2 minimum is reached in the fitting of the γ-ray line shape. The obtained angular distribution is then used for the simulation in gold. The iteration is continued until the convergence criteria are met (i.e., until the changes in the angular distribution and in the mean lifetime value are neglible within the statistical uncertainties).

When the level lifetime is short, this iterative procedure converges, yielding a unique lifetime value and an effective angular distribution, only if slowing-down materials with differing stopping powers (high and low) are used. On the other hand, if the level lifetime is about 100 fs or longer, the angular correlation and the slowing-down effects show up in different portions of the γ-ray line shape, and a single stopping material is sufficient for achieving convergence. Nevertheless, data from both Si and Au measurements were used for the iteration in all cases, except for the 3005- and 3264-keV levels. The lifetime values for these levels were based on the Si data only because the γ-ray line shapes were weak and contaminated in the Au data.

The stopping powers of the slowing-down media for ^{32}P ions were described in the DSA analysis according to the equation

$$\left(\frac{dE}{dx}\right)=\left(\frac{dE}{dx}\right)_e+\left(\frac{dE}{dx}\right)_n^{\mathrm{ZBL}}. \quad (1)$$

Because an experimentally verified electronic stopping power $(dE/dx)_e$ of gold for ^{31}P ions is unavailable, predicted stopping power values were taken from Ref. [38] for velocities $v \geq 2.45 v_0$ ($v_0=c/137$, where c is the velocity of light). The prediction is based on an interpolation of experimental data for ^{27}Al and ^{32}S ions using the effective charge formalism. For lower velocities, the electronic stopping power was extended linearly to zero at $v=0$. The electronic stopping power of silicon was obtained from Ref. [39]. The uncertainty in $(dE/dx)_e$ was $\pm 6\%$ for gold and $\pm 11\%$ for silicon. These uncertainties are reflected in the uncertainties quoted for the deduced lifetime values.

The nuclear stopping power $(dE/dx)_n$ was calculated by the MC method, where the scattering angles of the recoiling ions were derived directly from the classical scattering integral [27] and the interatomic interaction described by the universal Ziegler-Biersack-Littmark (ZBL) potential [40]. As shown in Ref. [41], the exact choice of potential is relatively unimportant when the recoil velocities are high as in the current case.

Except for the slowing-down process, most other aspects of the MC simulation can be checked by analyzing the line shape of an extremely fast transition. In this study, the ground-state transition from the 8.13-MeV level in ^{32}S ($\tau=0.23\pm0.03$ fs [34]) provided a built-in cross check of our analysis.

C. Reanalysis of the previous results

The lifetime results obtained in this work for levels in ^{32}P are summarized and compared with previously reported values in Table I. The DSA results from different lifetime measurements show wide variations. To understand these variations further, previous results were critically examined. In those cases for which sufficient details of the experimental setup, target structure, and $F(\tau)$ values are given, the data were reanalyzed using our MC-simulation techniques and the current knowledge of the stopping power. The resulting lifetimes are also listed in Table I. In some cases, these values are significantly different from published values. A short description of the essential points that were considered in the reanalysis is given below.

In four of the six previous DSA experiments, the targets consisted of relatively thick layers (several hundred nanometers) of SiO_2 evaporated on carbon or gold backings. The accuracy of short lifetimes ($\tau<100$ fs) obtained with layered

targets is limited because there are several possible sources of large systematical errors; in particular (i) the composition of the evaporated layer is not known, (ii) the density of target can differ considerably (up to 30%) from that of bulk material, and (iii) the thickness and homogeneity of the target are uncertain.

In vacuum evaporation of SiO_2, a chemical reduction takes place, and the ensuing deposited layer is a mixture of Si, SiO, and SiO_2, but the exact fractions are not known [42–44]. Properties of such films strongly depend on the conditions under which the deposition is carried out [45]. Composition of the evaporated film changes also during ion beam irradiation, SiO transforming to Si and SiO_2 [46]. The bulk densities of Si, SiO, and SiO_2 are between 2.18 and 2.65 g/cm^3 [47], but in vacuum-evaporated targets, these densities are seldom reached because deposited layers are often porous and thus of reduced density. Furthermore, ceramics such as oxides of silicon do not easily stick to gold [48].

The exact stoichiometry (i.e., the relative proportions of Si, SiO, and SiO_2 in the targets) or the density of the evaporated SiO_2 targets have not been critically examined in any of the previous DSA studies of ^{32}P levels. Uncertainties in the target composition translate into unknown variations in the target density and stopping power. Therefore, in the reanalysis, we assumed a density of 2.18 g/cm^3 with a $\pm 25\%$ uncertainty. In this way, the unknown composition and porous structure of evaporated SiO_2 targets are accounted for to a reasonable extent.

The target thicknesses are usually given as areal densities (in μg/cm^2), but in the case of layered targets, a more relevant unit would be nanometer. The uncertainty in the density of the target material is directly reflected in the uncertainty of the target thickness. The effect on the deduced lifetime values is especially important in cases for which the target and the backing materials have very different stopping powers and the slowing down of recoils takes place in both. There is also an uncertainty in the target thickness, independent of the density. If this uncertainty was not given in the original paper, we allowed for a $\pm 10\%$ thickness variation in the reanalysis.

An important source of uncertainty can also be the density of the backing material. Generally, we used the density value of bulk material in the reanalysis if a metallic backing was used. In the case of the thin evaporated carbon backing used in Ref. [5], we kept the density at the originally quoted value of 1.95 ± 0.15 g/cm^3—which is 87% of the bulk density of graphite.

In all previous DSA analyses, the nuclear stopping power was taken either directly from the Lindhard-Scharff-Schiøtt (LSS) theory [49] or from an analytic approximation of it. The large-angle scattering was described by the analytic expressions introduced by Blaugrund [50]. In some cases, even more simple approximations have been applied for the description of nuclear stopping power. These approximations are too crude when the recoil velocities are low and the slowing-down material has a considerably higher atomic number than the recoiling ion.

Excluding Ref. [11], in all previous DSA analyses, the electronic stopping power data were taken directly from the LSS theory or modified slightly with the help of experiments. Recent electronic stopping power data are not in contradiction with the older data at the velocities at which the previous measurements were performed.

Electronic stopping powers of carbon, phosphorus, silicon dioxide, and titanium for phosphorus ions were needed in the reanalysis. We used stopping power values of carbon, phosphorus, and oxygen based on the latest parametrization of the semiempirical model of Ziegler, Biersack, and Littmark [40,51], and assumed the values to be correct to within $\pm 10\%$. The predicted electronic stopping power of titanium for phosphorus was taken from Ref. [38] for velocities $v \geqslant 2.45 v_0$. For lower velocities, the stopping power was interpolated linearly to zero stopping at $v = 0$. The Bragg-Kleeman rule [52] was applied in calculations of the stopping power of the silicon dioxide compound, with the stopping power of silicon taken from Ref. [39]. It turned out, however, that the contribution to the stopping power from oxygen is relatively unimportant in the cases we tested because Si and SiO_2 (they are the extreme cases) yield identical $F(\tau)$ curves to within 1–2 % (assuming equal densities for Si and SiO_2). Thus, the uncertainty in the deduced lifetimes caused by the unknown oxygen content is negligibly small compared with other sources of error (especially density and stopping power uncertainties), and the reanalysis was performed assuming pure Si as a target material.

Excluding Ref. [11], all previous lifetime values were deduced from $F(\tau)$ values. Our work and Ref. [11] use γ-ray line-shape analysis to deduce the lifetimes. In cases of overlapping γ-ray peaks, the analysis of line shapes gives more reliable results than the analysis of peak centroids.

The lifetimes measured by the Utrecht group involved $p\gamma$-coincidence requirements in the ^{29}Si$(\alpha, p\gamma)$ reaction [5,8,9] and the ^{2}H$(^{31}$P$, p\gamma)$ reaction [11]. Therefore, their results are relatively unaffected by delayed feedings from higher-lying levels or contaminant peaks from other reaction channels. However, the uncertainties related to the target structure and composition remain. The lifetime values quoted originally in Refs. [5,8,9] were systematically shorter than our values. We believe that the main reason for this deviation is the use of bulk densities for the evaporated targets. If target densities are reduced by 20%, the revised lifetime values are about 10% longer than the original values, and in most cases the revised values agree with our results. The values from Ref. [8] (both originally quoted and reanalyzed) are systematically shorter. The reasons for the deviations could be the porosity of the silicon dioxide layer or voids between target and backing.

In the unpublished study by the Utrecht group [11], a target of evaporated titanium on gold, silver, or copper backing was used. Because the recoil velocities were relatively high, the slowing down of the beam or the recoils in the target layer were not included in the original analysis. This assumption was tested in the reanalysis by simulating the γ-ray line shapes for the levels studied in Ref. [11] and varying the thickness of the target layer. The effect of the target layer on the deduced lifetime values was observed to be relatively unimportant, except for the 1149-keV level, for which the reanalysis yielded a slightly longer lifetime. The uncertainties of the revised values were enlarged accordingly. This particular Utrecht study [11] is limited to just four levels below an excitation energy of 1.8 MeV in ^{32}P.

TABLE VI. Binding energy (in MeV) of the lowest-lying state in ^{32}P and excitation energies of other states relative to this energy as a function of the number of holes n in the $0d_{5/2}$ orbit. These excitation energies are also compared with the experimental energies.

J^π	$n=0$	$n=1$	$n=2$	$n=3$ [a]	full	exp.
1^+	-170.040	0.028	-174.539	-174.748	0.005	0.000
2^+	0.664	-171.772	0.178	0.167	-175.578	0.078
0^+	0.703	0.301	0.478	0.235	0.260	0.513
2^-	7.081	4.566	3.985	3.610		3.264
3^-	5.891	4.463	3.854	3.103		3.321
4^-	5.552	4.533	3.937	3.155		3.443
0^-	7.739	6.599	6.433	5.665		4.411

[a]For $n=3$, all configurations were included except those with three $0d_{5/2}$ holes and four $0d_{3/2}$ particles. In addition to the four negative-parity states listed here, other negative-parity states were calculated to lie at 4.494(1^-), 4.903(3^-), 4.996(2^-), 5.332(2^-), 5.393(4^-), 5.449(1^-), 5.570(4^-), 5.572(3^-), 5.752(2^-), 5.782(3^-), 5.962(4^-), 6.055(0^-), and 6.099(3^-).

Results by the Liverpool group are based on measurements of singles γ-ray spectra in the ^{29}Si$(\alpha,p\gamma)$ reaction [7]. Relatively thick SiO_2 targets on gold were used, but no information was given on how the targets were prepared or how the thicknesses were measured. In some cases, γ-ray peaks originating from levels in ^{32}S and ^{29}Si [produced in the ^{29}Si$(\alpha,n\gamma)$ and ^{29}Si(α,α') reactions, respectively] overlapped with the ^{32}P peaks, causing difficulties in the determination of the $F(\tau)$ values. For example, the mean lifetime of the 2.74-MeV level was determined from a 1.60-MeV γ ray, supposedly the 2.74 $\rightarrow$ 1.15 MeV transition. The branching ratio for this transition is, however, only 1.6 $\pm$ 0.3% (see Table IV), and the correct assignment would have been the 3.62 $\rightarrow$ 2.03 MeV transition ($E_\gamma=1596$ keV) in ^{29}Si. The 1149- and 1323-keV levels were reported to receive some delayed feeding, but because the feeding percentages were not given, the revised lifetime values given for them in Table I are upper limits. For other levels, the revised values are in good agreement with the current ones.

The $F(\tau)$ values given in Ref. [10] have large uncertainties because of apparent difficulties in determining the very small γ-ray-induced Doppler shifts in the ^{31}P(thermal $n,\gamma\gamma$) experiment. Assuming a value of 2.16 g/cm^2 for the density of the amorphous red phosphorus target used in Ref. [10], the reanalysis yielded lifetime values that are about 20% longer than the quoted ones. Within uncertainties, they are in agreement with our values.

In summary, our reanalysis of the previously published DSA data has yielded revised lifetime values that are, in most cases, in good agreement with the values measured in the current study. This fact also gives us some confidence on the revised lifetime values of levels that we were not able to populate in our current experiment with the ^{2}H$(^{31}$P$,p\gamma)$ reaction. The adopted lifetime values given in Table I were calculated as weighted averages of the reanalyzed values and our values. The only exception is the 3005-keV level, for which we disregarded the low value of 44 $\pm$ 13 fs. For each level, the uncertainty in the adopted lifetime value was kept the same as the uncertainty in the best reported value.

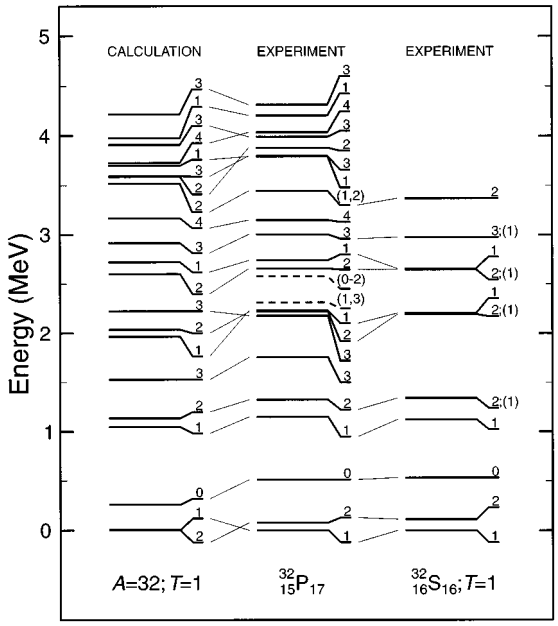

FIG. 2. Comparison of calculated and experimental level schemes for positive-parity $T=1$ states in ^{32}P and ^{32}S. The ^{32}S states are shifted down by 7003 keV, so that the lowest known $T=1$ state in ^{32}S coincides with the ground state of ^{32}P. The levels shown by dashed lines at 2313 and 2579 keV in ^{32}P are spurious. All experimental energies and $J^\pi;T$ assignments are from Ref. [34]. Uncertain assignments are given in parentheses.

III. CALCULATIONS

A. Procedure

Shell-model calculations of energy levels and γ-decay properties were performed for both positive- and negative-parity states in ^{32}P using the shell-model program OXBASH [53]. The wave functions for all positive-parity states were obtained by constructing all possible configurations within the major oscillator shell defined by the $0d_{5/2}$, $0d_{3/2}$, and $1s_{1/2}$ orbitals (*sd*-shell) and diagonalizing the effective Hamiltonian of Wildenthal [12]. The γ-decay properties for the positive-parity states were computed using harmonic oscillator radial wave functions with $\hbar\omega=(45A^{-1/3}-25A^{-2/3})$ MeV and effective $M1$ [13] and $E2$ [14] operators. The calculated branching and mixing ratios are given in Table IV, in which they are compared with the experimental values.

To account for negative-parity states, the model space must be extended beyond the *sd* shell to include $1\hbar\omega$ [one-particle, one-hole $(1p$-$1h)$] excitations into the next major shell—in particular, the $0f_{7/2}$, $0f_{5/2}$, $1p_{3/2}$, and $1p_{1/2}$ orbitals (*fp*-shell). The effective Hamiltonian was chosen to be the Warburton-Becker-Millener-Brown (WBMB) *sd-fp* shell Hamiltonian described in Ref. [54]. The WBMB Hamiltonian consists of the Wildenthal matrix elements for the *sd*-shell, McGrory's *fp*-shell Hamiltonian for the *fp*-shell matrix elements [55], and a modification of the Millener-Kurath interaction for the cross-shell components [56]. Consequently, in the *full sd-fp* shell-model space, the $0\hbar\omega$

TABLE VII. Comparison of experimental and calculated level energies and lifetimes in ^{32}P.

E_x^{exp} (keV)	E_x^{calc} (keV)	J^π	τ(fs) exp.	τ(fs) calc. [a]
0	5	1_1^+		
78	0	2_1^+	402 *13* ps	310 ps
513	260	0_1^+	2.64 *12* ps	2.03 ps
1149	1047	1_2^+	264 *18*	348
1323	1135	2_2^+	487 *25*	406
1755	1528	3_1^+	621 *40*	152
2178	2224	3_2^+	76 *14*	321
2218	2036	2_3^+	240 *25*	43.1
2230	1965	1_3^+	$<$50	58.1
2657	2602	2_4^+	12 *4*	13.2
2740	2722	1_4^+	20 *7*	31.8
3005	2916	3_3^+	101 *16*	221
3149	3168	4_1^+	595 *110*	104
3264	3610	2_1^-	164 *22*	25
3321	3103	3_1^-	272 *50*	460
3443	3155	4_1^-	0.387 *45* ps	12.81 ps
3444	3518	2_5^+	38 *15*	24.5
3792	3697	1_5^+	5.7 *20*	3.9
3797	3592	3_4^+	77 *43*	6.1
3880	3587	2_6^+	$<$20	5.5
3990	3909	3_5^+	$<$15	7.0
4009	4996	2_2^-	188 *40*	6.5
4035	3727	4_2^+	45 *30*	25.4
4036	4494	1_1^-	2.1 *8*	6.2
4151	4903	3_2^-	30 *10*	78
4205	3976	1_6^+	4.2 *11*	2.5
4313	4217	3_6^+	90 *50*	10.1
4411	5665	0_1^-	19 *3*	0.9
4743	4977	5_1^+	160 *70*	133
4877	5449	1_2^-	5.7 *11*	6.4

[a]Lifetimes for the negative-parity states are calculated using the model space with three holes allowed in the $0d_{5/2}$ orbit, as discussed in the text. The following lifetimes are obtained if two holes are allowed: $\tau(3264) = 41$ fs, $\tau(3321) = 2.430$ ps, $\tau(3443) = 2.660$ ps, $\tau(4009) = 14.7$ fs, $\tau(4036) = 6.4$ fs, $\tau(4151) = 50$ fs, $\tau(4411) = 5.8$ fs, and $\tau(4877) = 3.5$ fs.

positive-parity states are the same as those in the *sd*-shell calculations described above.

Negative-parity states arise not only from *sd*-to-*fp* excitations but also from $1p$-$1h$ excitations out of the closed ^{16}O core (i.e., the $0p_{3/2}$ and $0p_{1/2}$ orbits) into the *sd* shell. Because the $0d_{5/2}$ orbit is essentially filled, these $1p$-$1h$ excitations should be at a higher excitation energy than their *sd*-to-*fp* shell counterparts. This observation is at least partially confirmed by noting that the lowest negative-parity state in the $T_z = \pm 1/2$, $A = 29$–33 nuclides has $J^\pi = 7/2^-$. Thus, the low-lying negative-parity states in ^{32}P are most likely dominated by $1p$-$1h$ *sd*-to-*fp* shell excitations.

Unlike the positive-parity states, the number of states with definite angular momentum and isospin (J,T dimensions) associated with the negative-parity states is on the order of 30 000–50 000, and is prohibitively large. For this reason, some model-space truncations were required. These truncations were based primarily on the number of holes n permitted in the $0d_{5/2}$ orbit. The properties of the negative-parity states were examined for both $n=2$ and $n=3$. For the $n=3$ case, all configurations were included, except those consisting of three $0d_{5/2}$ holes and four $0d_{3/2}$ particles. These basis states were excluded because of difficulties encountered while projecting angular momentum and isospin with the shell-model program OXBASH. The largest J,T dimension encountered in the calculations was 16 606, which occured for $J^\pi;T = 3^-;1$.

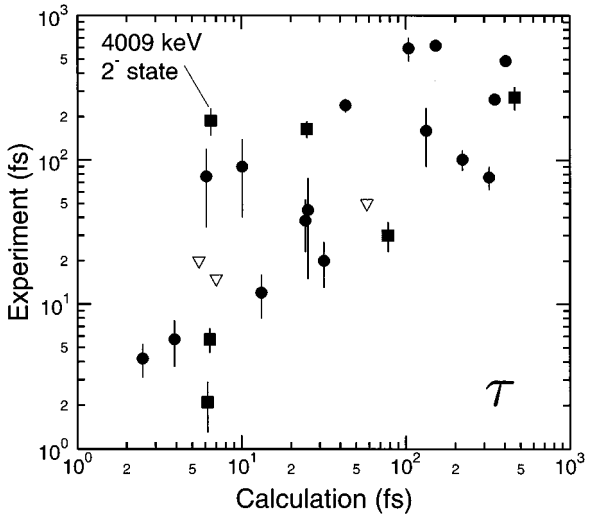

FIG. 3. Calculated mean lifetimes compared to those experimentally determined. Positive-parity states are shown by circles and negative-parity states by squares. Experimental upper limits are shown by open triangles. Calculated lifetimes agree with experiment to within a factor of 5 inside the shaded region.

Currently, no reliable information exists regarding effective charges for the computation of $E1$ transition matrix elements in this mass region. Therefore, bare proton and neutron charges (including corrections resulting from the center-of-mass motion [57]) were used. The calculated branchings of negative-parity states are given in Table V, in which they are compared with experimental results. In addition, the positive-parity states were also obtained by requiring the same truncation on the *sd*-shell configurations. It was found that the low-lying positive-parity states had an overlap with the corresponding full-space wave functions of better than 89 and 93 % for the $n=2$ and 3 cases, respectively. Hence, the truncations used are probably adequate in a test of the shell-model interaction for transition amplitudes.

It is, however, somewhat difficult to predict with an accuracy of better than $\sim$0.5 MeV the excitation energies of the negative-parity states relative to the positive-parity states. This difficulty arises because (i) the negative-parity states do not contain the complete *sd*-shell excitations and (ii) the same truncation applied to positive- and negative-parity states contains different levels of completeness. This effect is illustrated in Table VI, which shows the shell-model binding and excitation energies of the lowest positive- and negative-parity states tabulated as a function of n and compared with experimental energies. Generally speaking, we note an overall reduction, and apparent convergence, in the excitation energies of the negative-parity states with $n=3$. In addition,

TABLE VIII. Comparison of experimental and calculated reduced $M1$ and $E2$ transition probabilities for transitions between positive-parity states in ^{32}P.

Initial state		Final state		$B(M1)$ (W.u.)		$B(E2)$ (W.u.)	
E_x (keV)	J^π	E_x (keV)	J^π	exp.	calc.	exp.	calc.
513	0_1^+	0	1_1^+	0.089 *3*	0.116		
1149	1_2^+	78	2_1^+	0.041 *3*	0.00036	3.0 *29*	0.041
		513	0_1^+	0.23 *2*	0.349		
1755	3_1^+	0	1_1^+			0.27 *7*	0.0038
		78	2_1^+	0.0064 *5*	0.0375	6.1 *9*	8.92
		1323	2_2^+	0.0125 *11*	0.0583	4.1 $^{70}_{40}$	0.053
2178	3_2^+	0	1_1^+			3.3 *7*	4.74
		78	2_1^+	0.040 *7*	0.0037	0.76 *35*	0.475
2218	2_3^+	0	1_1^+	0.0052 *10*	0.0035	1.1 *7*	2.71
		1323	2_2^+	0.044 *5*	0.0810	$<$21.7	2.10
2657	2_4^+	0	2_1^+	0.09 2	0.0602	1.7 *8*	0.335
2740	1_4^+	513	0_1^+	0.10 *4*	0.0328		
3005	3_3^+	0	1_1^+			0.37 *7*	0.531
		1323	2_2^+	0.0007 *5*	0.0034	3.3 *10*	1.61
		2178	3_2^+	0.022 *4*	0.0073	1.7 $^{50}_{14}$	6.93
3149	4_1^+	78	2_1^+			0.059 *11*	0.501
		1323	2_2^+			6.7 *12*	5.571
		1755	3_1^+	0.00011 *6*	0.0776	5.5 *11*	8.09
		2178	3_2^+	0.012 *2*	0.0305	0.6 *5*	0.781
3444	2_5^+	513	0_1^+			1.2 *5*	0.447
3797	3_4^+	78	2_1^+	0.0013 *9*	0.0631	0.14 $^{19}_{13}$	0.527
		1323	2_2^+	0.021 *12*	0.0988	$<$0.02	1.24
4035	4_2^+	78	2_1^+			1.1 *7*	4.18
		1755	3_1^+	0.039 *26*	0.0091	$<$0.05	0.585
4743	5_1^+	2178	3_2^+			2.2 *10*	2.91
		3005	3_3^+			6.5 *29*	5.51
		3149	4_1^+	0.023 *10*	0.0296	0.55 *43*	0.402
		4035	4_2^+	0.069 *30*	0.0561	0.5 $^{18}_{4}$	0.011

both the overall structure of the negative-parity spectrum and the computed $B(E1)$ values are generally unchanged between the $n=2$ and $n=3$ calculations.

In shell-model calculations, the spurious center-of-mass (SCOM) states are removed usually by adding a center-of-mass Hamiltonian with a large coupling constant to the shell-model Hamiltonian, as was done in this work, which then pushes the SCOM states up to a high excitation energy. This procedure completely removes the spurious states only when the full $1\hbar\omega$ space is used. Our calculations for the negative-parity states did not use the full $1\hbar\omega$ space. To test the level of spuriosity, transition matrix elements of the SCOM raising operator defined by [58]

$$B_\mu^\dagger = \frac{1}{\sqrt{2mA\hbar\omega}} \sum_{k=1}^{A} [-i(p_k)_\mu + m\omega(r_k)_\mu] \qquad (2)$$

were computed between the lowest positive- and negative-parity states. Usually, the square of the reduced matrix elements of $B_\mu^\dagger$ were found to be less than 10^{-7}, indicating that the level of spuriosity in the lowest negative-parity states is small enough such as not to be a major concern.

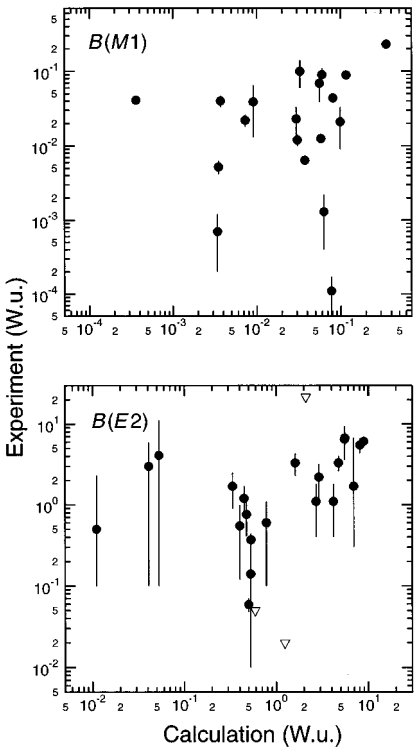

FIG. 4. Comparison of calculated and experimental reduced transition probabilities: $B(M1)$ (upper); $B(E2)$ (lower). Experimental upper limits are shown by open triangles. Calculated values agree with experiment to within a factor of 5 inside the shaded region.

B. Results

As shown in Fig. 2, the correspondence between predicted and experimentally observed positive-parity states in ^{32}P is very good up to an excitation energy of 4.3 MeV. Above this energy, the level density is high, and the experimental spectrum contains many uncertainties. Therefore, it becomes difficult to establish a one-to-one correspondence between theory and experiment. A notable success of the predictions is that the two suggested levels at 2313 and 2579 keV are missing from the predicted spectrum. Indeed, it has been shown that the γ rays reported in the ^{31}P(thermal n,γ) reaction [59] that led to these levels are spurious [35].

The predicted level stucture for negative-parity states is compared only for the few lowest states of each angular momentum (see Tables VI and VII). As was explained in the previous section, an accuracy of approximately 0.5 MeV can be achieved at best. Given this limitation, it is encouraging to note that the lowest negative-parity states are predicted to lie very near each other in energy, a feature that is also observed in the experimental spectrum. The gap between the three lowest states and other states is reproduced, although the width of the gap is exaggerated. The higher lying negative-parity states cannot be confidently matched with experimental levels.

To test the calculations further, electromagnetic decay properties were also examined. Because only 16 $E2/M1$ mixing ratios for positive-parity states and 6 $M2/E1$ mixing ratios for negative-parity states are experimentally known, we have chosen to compare calculated lifetimes with the experimental ones. These comparisons are reported in Table VII and Fig. 3. Except for the 4009-keV, 2^- state for which the calculated lifetime is $\sim$1/30 of the measured value, all other calculated lifetimes agree with measurements to within a factor of $\sim$5, as shown in Fig. 3. The predicted values tend to be slightly shorter.

In the cases for which the mixing ratio is known experimentally or the transition is of pure multipole, we have shown in Table VIII a comparison of the experimental reduced transition probability with the calculated value. In the calculation of predicted lifetimes (see Table VII), experimental energies were used. From these lifetimes and the calculated branching ratios and mixing ratios shown in Table IV, the individual transition strengths or matrix elements can be deduced as more mixing ratios become available.

The experimental and predicted reduced transition probabilities shown in Fig. 4 are also in fairly good agreement. For the most part, it is found that $E2$ transitions in the $\sim$0.5–10 W.u. range are predicted correctly. As in the $E2$ case, the strongest $M1$ transitions are also quite well predicted, but the weaker transitions sometimes show quite large variations when compared to the experimental results.

The comparison between the measured and calculated lifetimes for the two lowest 3^+ states at 1755 and 2178 keV (see Table VII) suggest that the order of these two states appears inverted in the predicted spectrum. This assumption, however, is not supported by the calculated branching and mixing ratios (see Table IV), which, for the 1755-keV state, are in good agreement with experiments. For the 2178-keV state, the calculated branching and mixing ratios are not in as good agreement with experiments as for the 1755-keV state. From Table VIII, one can see that for the 1755-keV state, the predicted $B(M1)$ values are overestimated by a factor of 5, while the predicted $B(E2)$ values are rather good. For the 2178-keV state, the $B(M1)$ value for the transition to the 78-keV state is underestimated by a factor of 10, while its $B(E2)$ value and that for the transition to the ground state are correctly predicted. Also, the lifetimes of the third and fifth 3^+ states are poorly reproduced (see Table VII), but again the branching and mixing ratios (see Table IV) are reasonable.

In contrast to the positive-parity states, the agreement between theory and experiment for the lifetimes of the negative-parity states is poor (see Table VII). For the most part, the $E1$ transitions studied here are rather weak (as is also predicted by the calculations), and thus are sensitive to details of the shell-model wave functions—in particular to cancellations between the various components. Usually, weaker transitions are difficult to reproduce in any shell-model calculation, as is also apparent from comparisons for the $E2$ and $M1$ transitions described previously. With regard to the influence of the model-space truncations, the $B(E1)$ transitions are of similar magnitude in the $n=2$ and $n=3$ calculations (see Table IX). The most glaring exception involves the first 0^- state, for which not only does the $B(E1)$ value for the ground-state transition change by three orders of magnitude, but also this is the largest $B(E1)$ value computed. This large change in the $E1$ strength arises because in both $n=2$ and $n=3$ calculations the two lowest 0^- states are split by only a few hundred keV and in the $n=2$ case the $E1$ strength is concentrated to the higher en-

TABLE IX. Comparison of experimental and calculated reduced $E1$ transition probabilities in ^{32}P. The two different calculations ($n=2$ or $n=3$, respectively, is the number of holes in the $0d_{5/2}$ orbit) are described in the text. In our notation 2.85−6 W.u. ≡ $(2.8 \pm 0.5)\times 10^{-6}$ W.u.

Initial state		Final state		$B(E1)$ (W.u.)		
E_x (keV)	J^π	E_x(keV)	J^π	exp.	$n=2$	$n=3$
3264	2_1^-	0	1_1^+	2.7 *5*−6 [a]	7.1−7	2.6−4
		78	2_1^+	2.3 *3*−5	7.0−4	8.2−4
		1149	1_2^+	3.0 *4*−4 [a]	8.8−5	2.9−4
		1323	2_2^+	1.3 *3*−4 [a]	2.9−8	3.2−6
		1755	3_1^+	2.2 *3*−4	1.2−5	9.2−5
		2230	1_3^+	4.5 *6*−4	3.5−5	1.4−4
3321	3_1^-	78	2_1^+	7.8 *15*−5 [a]	7.7−6	6.0−5
		1323	2_2^+	1.1 *2*−4	1.4−5	2.2−11
3443	4_1^-	1755	3_1^+	4.9 *6*−4 [a]	3.1−6	2.9−6
		2178	3_2^+	7.4 *17*−5 [a]	1.7−4	2.3−5
4009	2_2^-	0	1_1^+	2.2 *5*−5	7.0−4	2.0−3
		78	2_1^+	2.1 *5*−5	2.3−4	1.4−4
		1149	1_2^+	1.3 *3*−5	5.7−5	3.1−4
		1323	2_2^+	1.8 *4*−5	7.2−5	2.3−5
		1755	3_1^+	3.1 *7*−5	1.2−4	2.3−4
		2178	3_2^+	1.6 *4*−5	1.5−6	1.5−5
		2218	2_3^+	1.8 *5*−5	1.1−4	8.6−8
		2657	2_4^+	4.5 *12*−5	1.7−5	1.1−4
		3005	3_3^+	7.1 *18*−5	3.1−6	2.3−4
		3444	2_5^+	3.4 *9*−4		
4036	1_1^-	0	1_1^+	1.6 *6*−5	2.8−4	3.1−5
		78	2_1^+	2.4 *9*−4	1.6−4	2.2 −6
		513	0_1^+	7.1 *27*−3	2.1−3	2.6−3
		1149	1_2^+	4.0 *16*−3	1.2−3	1.5−3
		1323	2_2^+	3.5 *14*−4	4.6−6	1.1−5
		2230	1_3^+	2.9 *13*−3	3.5−4	3.8−4
		2657	2_4^+	3.2 *15*−3	3.4−4	3.7−4
4151	3_2^-	78	2_1^+	3.3 *11*−4 [a]	1.8−4	1.1−4
		1755	3_1^+	1.1 *5*−4	8.0−5	1.1−4
		2218	2_3^+	3.1 *15*−4	2.6−4	7.7−5
		2657	2_4^+	1.2 *5*−3	3.1−6	2.0−8
4411	0_1^-	0	1_1^+	5.2 *8*−4	4.3−5	1.3−2
		1149	1_2^+	1.9 *4*−4	4.6−3	3.8−4
4877	1_2^-	0	1_1^+	1.4 *3*−4	2.2−4	1.9−6
		78	2_1^+	4.3 *9*−5	9.5−5	5.7−4
		513	0_1^+	1.4 *3*−3	1.9−3	5.1−4
		1323	2_2^+	3.1 *6*−4	1.8−5	4.3−5
		2740	1_4^+	7.0 *17*−4	2.8−3	2.2−3
		3444	2_5^+	1.2 *4*−3	1.53−6	

[a]The $M2/E1$ mixing ratios are from Ref. [34].

ergy state, while in the $n=3$ case the $E1$ strength is more evenly distributed between the two states. The summed strengths of the two states are roughly equal in both calculations. For the most part, no definitive conclusions regarding effective charges for the $E1$ operator can be drawn from the current study, although it would be interesting to investigate a situation for which a full $1\hbar\omega$ calculation could be performed.

IV. SUMMARY

Lifetime values have been measured for 26 bound levels out of ~70 known levels below the excitation energy of 6.4 MeV in ^{32}P. The results based on experimental stopping power in the DSA analysis and realistic MC simulations of the experimental conditions remove the large uncertainty of the lifetime values of excited ^{32}P levels reported in the literature. Shell-model calculations are able to reproduce the measured lifetimes to a reasonable degree. Also, the electromagnetic transition strengths are in most cases predicted correctly. A more detailed comparison, especially for levels above 4.9 MeV, requires additional information such as unambiguous J^π assignments and data on $E2/M1$ mixing ratios.

ACKNOWLEDGMENTS

This work was sponsored, in part, by the Academy of Finland and, in part, by the U.S. Department of Energy under Contract No. DE-AC05-96OR22464 with Lockheed Martin Energy Research Corporation (Oak Ridge).

[1] A. Burkard, G. Glatz, M. Lickert, T. Kern, R. Lehmann, S. Norbert, H. Röpke, J. Siefert, and B. H. Wildenthal, Z. Phys. A **324**, 173 (1986).
[2] P. Tikkanen, J. Keinonen, A. Kangasmäki, Zs. Fülöp, Á. Z. Kiss, and E. Somorjai, Phys. Rev. C **47**, 145 (1993).
[3] R. A. Mendelson, Jr. and R. T. Carpenter, Phys. Rev. **165**, 1214 (1968).
[4] J. F. Boulter and W. V. Prestwich, Can. J. Phys. **48**, 868 (1970).
[5] G. van Middelkoop and C. J. Th. Gunsing, Nucl. Phys. **A147**, 225 (1970).
[6] D. M. Gordon and R. W. Kavanagh, Phys. Rev. C **4**, 145 (1971).
[7] P. E. Carr, D. C. Bailey, L. L. Green, A. N. James, J. F. Sharpey-Schafer, and D. A. Viggars, J. Phys. A **6**, 705 (1973).
[8] F. E. H. van Eijkern, G. van Middelkoop , J. Timmer, and J. A. van Luijk, Nucl. Phys. **A210**, 38 (1973). The signs of the mixing ratios given in Table 3 of this paper should be changed as explained on p. 133 of Ref. [9].
[9] F. E. H. van Eijkern, G. van Middelkoop, W. A. Sterrenburg, and A. F. C. Buijense, Nucl. Phys. **A260**, 124 (1976).
[10] Y. E. Koshutskii, V. T. Kupryashkin, N. V. Stril'chuk, A. I. Feoktistov, and I. P. Shapovalova, Izv. Akad. Nauk. SSSR, Ser. Fiz. 54, 844 (1990) [Bull. Acad. Sci. USSR, Phys. Ser. **54**, 27 (1990)].
[11] E. J. Evers, C. Anderliesten, R. J. Elsenaar, E. J. van der Kley, D. L. Verhoff, and C. van der Leun (unpublished).
[12] B. H. Wildenthal, in *Progress in Particle and Nuclear Physics*, edited by D. H. Wilkinson (Pergamon, Oxford, 1984), Vol. 11, p. 5.
[13] B. A. Brown and B. H. Wildenthal, Nucl. Phys. **A474**, 290 (1987).
[14] B. A. Brown and B. H. Wildenthal, Annu. Rev. Nucl. Part. Sci. **38**, 29 (1988).
[15] J. Keinonen, V. Karttunen, J. Räisänen, F.-J. Bergmeister, A. Luukkainen, and P. Tikkanen, Phys. Rev. B **34**, 8981 (1986).
[16] A. Kehrel, J. Keinonen, P. Haussalo, K. P. Lieb, and M. Uhrmacher, Radiat. Eff. **118**, 297 (1991).
[17] P. Haussalo, J. Keinonen, U. M. Jäske, and J. Sievinen, J. Appl. Phys. **75**, 7770 (1994).
[18] A. Anttila, M. Bister, A. Luukkainen, Á. Z. Kiss, and E. Somorjai, Nucl. Phys. **A385**, 194 (1982).
[19] Y. Yoshizawa, Y. Iwata, T. Kaku, T. Katoh, J. -Z. Ruan, T. Kojima, and Y. Kawada, Nucl. Instrum. Methods **174**, 109 (1980).
[20] M. Hautala, A. Anttila, and J. Keinonen, Nucl. Instrum. Methods **150**, 599 (1978).
[21] W. H. Trzaska, Nucl. Instrum. Methods Phys. Res. A **297**, 223 (1990).
[22] M. E. Phelps, D. G. Sarantites, and W. G. Winn, Nucl. Phys. **A149**, 647 (1970).
[23] D. C. Camp and G. L. Meredith, Nucl. Phys. **A166**, 349 (1971).
[24] G. J. McCallum and G. E. Coote, Nucl. Instrum. Methods **124**, 309 (1975).
[25] G. J. Schmid, R. M. Chasteler, C. M. Laymon, H. R. Weller, E. F. Moore, C. R. Bybee, J. M. Drake, D. R. Tilley, G. Vavrina, and P. M. Wallace, Nucl. Phys. **A607**, 139 (1996).
[26] B. Krusche, K. P. Lieb, H. Daniel, T. von Egidy, G. Barreau, H. G. Börner, R. Brissot, C. Hofmeyr, and R. Rascher, Nucl. Phys. **A386**, 245 (1982). The γ-ray energies listed in Table 2 of this paper are uncorrected for recoil even though the footnote states otherwise.
[27] J. Keinonen, in *Capture Gamma-ray Spectroscopy and Related Topics*, Knoxville, Tennessee, Proceedings of the Fifth International Symposium on Capture Gamma-ray Spectroscopy and Related Topics, edited by S. Raman, AIP Conf. Proc. No. 125 (AIP, New York, 1985), p. 557.
[28] P. Tikkanen, J. Keinonen, V. Karttunen, and A. Kuronen, Nucl. Phys. **A456**, 337 (1986).
[29] P. Tikkanen, J. Keinonen, R. Lappalainen, and B. H. Wildenthal, Phys. Rev. C **36**, 32 (1987).
[30] J. Keinonen, P. Tikkanen, A. Kuronen, Á. Z. Kiss, E. Somorjai, and B. H. Wildenthal, Nucl. Phys. **A493**, 124 (1989).
[31] P. Tikkanen, J. Keinonen, K. Arstila, A. Kuronen, and B. H. Wildenthal, Phys. Rev. C **42**, 581 (1990).
[32] P. Tikkanen, J. Keinonen, A. Kuronen, Á. Z. Kiss, E. Koltay, É. Pintye, and B. H. Wildenthal, Nucl. Phys. **A517**, 176 (1990).
[33] P. Tikkanen, J. Keinonen, A. Kangasmäki, Zs. Fülöp, Á. Z. Kiss, and E. Somorjai, Phys. Rev. C **43**, 2162 (1991).
[34] P. M. Endt, Nucl. Phys. **A521**, 1 (1990).
[35] E. T. Jurney and J. W. Starner (private communication).
[36] W. J. Stark, P. M. Cockburn, and R. W. Krone, Phys. Rev. C **1**, 1752 (1970).
[37] E. J. Hoffman, D. M. van Patter, D. G. Sarantites, and H. J. Barker, Nucl. Instrum. Methods **109**, 3 (1973).
[38] J. S. Forster, D. Ward, H. R. Andrews, G. C. Ball, G. J. Costa, W. G. Davies, and I. V. Mitchell, Nucl. Instrum. Methods **136**, 349 (1976).

[39] J. Keinonen, K. Arstila, and P. Tikkanen, Appl. Phys. Lett. **60**, 228 (1992).
[40] J. F. Ziegler, J. P. Biersack, and U. Littmark, in *The Stopping and Range of Ions in Solids*, edited by J. F. Ziegler (Pergamon, New York, 1985), Vol. 1.
[41] K. Arstila, J. Keinonen, and P. Tikkanen, Nucl. Instrum. Methods Phys. Res. B **101**, 321 (1995).
[42] A. C. Wolff, M. A. Mayer, and P. M. Endt, Nucl. Phys. **A107**, 332 (1968).
[43] P. R. Gardner, C. E. Moss, R. H. Spear, and L. E. Carlson, Aust. J. Phys. **25**, 659 (1972).
[44] J. D. MacArthur, S. -P. Kwan, H. -B. Mak, W. McLatchie, S. A. Page, S. -S. Wang, and T. K. Alexander, Phys. Rev. C **32**, 314 (1985).
[45] F. Rochet, G. Dufour, H. Roulet, B. Pelloie, J. Perrière, E. Fogarassy, A. Slaoui, and M. Froment, Phys. Rev. B **37**, 6468 (1988).
[46] D. Rodichev, Ph. Lavallard, E. Dooryhée, A. Slaoui, J. Perrière, M. Gandais, and Y. Wang, Nucl. Instrum. Methods Phys. Res. B **107**, 259 (1996).
[47] *CRC Handbook of Chemistry and Physics*, 76th ed., edited by D. R. Lide (CRC Press, Inc., Boca Raton, 1995), p. 4–82.
[48] R. Lappalainen and P. Torri (private communication).
[49] J. Lindhard and M. Scharff, Mat. Fys. Medd. K. Dan. Vidensk. Selsk. **27** (15), 1 (1953); J. Lindhard, *ibid.* **28** (8), 1 (1954); J. Lindhard and M. Scharff, Phys. Rev. **124**, 128 (1961); J. Lindhard, M. Scharff, and H. E. Schiøtt, Mat. Fys. Medd. K. Dan. Vidensk. Selsk. **33** (14), 1 (1963).
[50] A. E. Blaugrund, Nucl. Phys. **88**, 501 (1966).
[51] J. F. Ziegler (private communication).
[52] W. H. Bragg and R. Kleeman, Philos. Mag. **10**, 318 (1905).
[53] B. A. Brown, A. Etchegoyen, and W. D. M. Rae, computer code OXBASH, the Oxford-Buenos Aires-MSU shell model code, Michigan State University Cyclotron Laboratory, Report No. 524, 1985 (unpublished).
[54] E. K. Warburton, J. A. Becker, and B. A. Brown, Phys. Rev. C **41**, 1147 (1990).
[55] J. B. McGrory, Phys. Rev. C **8**, 693 (1973).
[56] D. J. Millener and D. Kurath, Nucl. Phys. **A255**, 315 (1975).
[57] P. J. Brussaard and P. W. M. Glaudemans, *Shell-Model Applications in Nuclear Spectroscopy* (North Holland, Amsterdam, 1977), p. 186.
[58] R. D. Lawson, *Theory of the Nuclear Shell Model* (Clarendon Press, Oxford, 1980), p. 225.
[59] S. Michaelsen, Ch. Winter, K. P. Lieb, B. Krusche, S. Robinson, and T. von Egidy, Nucl. Phys. **A501**, 437 (1989).